Coupling mid-infrared light from a photonic crystal waveguide to metallic transmission lines

Andrea Blanco-Redondo, Paulo Sarriugarte, Angel Garcia-Adeva, Joseba Zubia, and Rainer Hillenbrand

Coupling mid-infrared light from a photonic crystal waveguide to metallic transmission lines

Andrea Blanco-Redondo,[1,2,a)] Paulo Sarriugarte,[3] Angel Garcia-Adeva,[4] Joseba Zubia,[2] and Rainer Hillenbrand[3,5,a)]

[1]ICT-European Software Institute Division, Tecnalia, Ibaizabal Bidea, Ed. 202, 48170 Zamudio, Bizkaia, Spain
[2]Dpto. Electronica y Telecom., E.T.S. Ingeniería Bilbao, UPV/EHU, Alda. Urquijo, 48103 Bilbao, Bizkaia, Spain
[3]Nanooptics Group, CIC nanoGUNE Consolider, 20018 Donostia–San Sebastian, Gipuzkoa, Spain
[4]Dpto. Fisica Aplicada I, E.T.S. Ingeniería de Bilbao, UPV-EHU, Alda. Urquijo, 48103 Bilbao, Bizkaia, Spain
[5]IKERBASQUE, Basque Foundation for Science, 48011 Bilbao, Bizkaia, Spain

We propose and theoretically study a hybrid structure consisting of a photonic crystal waveguide (PhC-wg) and a two-wire metallic transmission line (TL), engineered for efficient transfer of mid-infrared (mid-IR) light between them. An efficiency of 32% is obtained for the coupling from the transverse magnetic (TM) photonic mode to the symmetric mode of the TL, with a predicted intensity enhancement factor of 53 at the transmission line surface. The strong coupling is explained by the small phase velocity mismatch and sufficient spatial overlapping between the modes. This hybrid structure could find applications in highly integrated mid-IR photonic-plasmonic devices for biological and gas sensing, among others. © 2014 Author(s). All article content, except where otherwise noted, is licensed under a Creative Commons Attribution 3.0 Unported License. [http://dx.doi.org/10.1063/1.4859635]

The concept of the integrated photonic chip is gaining momentum thanks to its promise to enable extremely compact, ultra-fast, and low-power consuming devices for a wide range of applications, from future optical interconnects[1,2] to biological sensing,[3,4] photon transistors,[5] and many others.[6] While conventional dielectric photonic waveguides enable low-loss light guiding through relatively long integrated circuits, photonic crystal waveguides provide further compactness[7] and control on the spatial, temporal, and spectral course of photons,[8] increasing the available on-chip functionality. Moreover, the state-of-the-art fabrication techniques have demonstrated light guiding in PhC-wgs with propagation loss as low as 2–4 dB/cm.[9–11] Yet, in terms of light confinement and thus compactness, plasmonic waveguides,[12–15] capable of beating the diffraction limit by orders of magnitude, are superior, turning them into exceptional platforms for nanosensing. Unfortunately, this extreme mode confinement comes at the expense of a very short propagation length.[16] It therefore appears that dielectric waveguides and PhC-wgs may become crucial components to guide optical signals through comparatively long spans in photonic chips, while plasmonic waveguides will play a key role confining those signals in the nanoscale domain. Consequently, with a view set on integrated photonic chips, it is important to provide an efficient coupling scheme between these two waveguide technologies.[17–19] Whereas several works have explored coupling from conventional dielectric waveguides to plasmonic waveguides,[20–26] here we propose and theoretically study a hybrid structure for coupling the modes of a PhC-wg to a two-wire metallic transmission line.

Photonic circuits in the mid-IR spectral range, from 3 to 10 μm, are relatively unexplored when compared to the work done in the visible and near-IR regions. The mid-IR range is, however, highly interesting for chemical and gas sensing, since photon energies here match well with molecular vibrations. Infrared spectroscopy is thus a powerful tool for chemical analysis but it is typically based on traditional, large instrumentation. Since miniaturization could come with mid-IR photonic circuits based on the integration of PhC-wgs and plasmonic waveguides,[15,27–30] we chose to explore coupling in this attractive spectral regime.

Fig. 1(a) shows the hybrid structure proposed here, consisting of a two-wire gold TL on top of a silicon PhC-wg. Two-wire transmission lines have recently proved their usefulness for guiding surface waves in the mid-IR, in the transition regime between strong plasmonic and practically perfect metallic behavior.[15,31] We study a two-wire TL, instead of a single metal wire or slab, as it represents a more flexible platform. The two-wire TL supports two different modes, symmetric and antisymmetric, with different mode volumes and propagation lengths, which allow us to selectively choose which mode to excite depending on the targeted application.[32,33] In parallel, silicon is now starting to be regarded as a promising material for the mid-IR,[34] and photonic crystals based on Si appear as a strong alternative to develop integrated photonic elements in this spectral region.[35] In this work, we focus on the coupling from the TM-like mode of the silicon PhC-wg to the symmetric mode of the TL.

In order to obtain efficient coupling of light with free-space wavelength of $\lambda_0 = 10 \, \mu$m between the PhC-wg and the TL, we designed an architecture that support modes of similar effective mode index, following the well-known principle of directional coupling.[36] The PhC structure is formed by a

a)Authors to whom correspondence should be addressed. Electronic addresses: andrea.blanco@tecnalia.com and r.hillenbrand@nanogune.eu
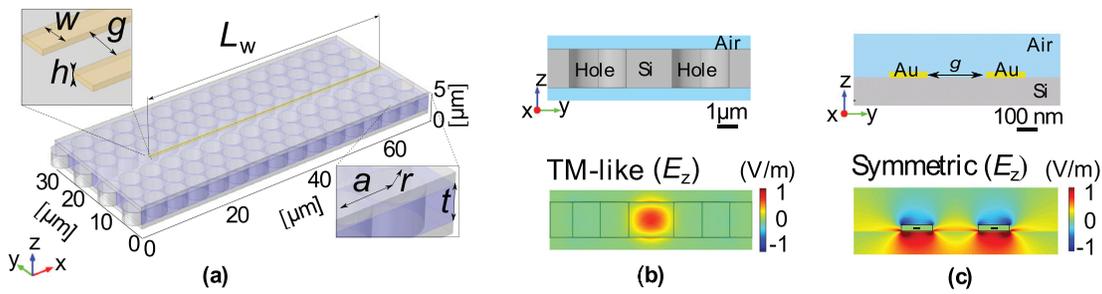
FIG. 1. Schematic of the proposed hybrid structure and the individual modes. (a) Photonic crystal waveguide is on a silicon slab ($a = 4.9\,\mu m$; $r = 0.48\,a$; $t = 0.6\,a$; $n_{Si} = 3.46$ and $n_{air} = 1$ at $\lambda_0 = 10\,\mu m$) with the transmission line on top consisting of two parallel gold wires ($w = 200\,nm$, $h = 40\,nm$, $L_w = 60\,\mu m$, $g = 300\,nm$; $n_{Au} = 12.59 + i\,59$ at $\lambda_0 = 10\,\mu m$). (b) Normalized real part of the electric field z-component (E_z) for the TM-like mode at $\lambda_0 = 10\,\mu m$ ($\omega_0 = a/\lambda_0 = 0.49$) in the PhC-wg. (c) Normalized real part of E_z for the symmetric mode in the TL on a silicon substrate.

hexagonal lattice of holes on a silicon slab, in which a central row of holes has been removed to form a waveguide, as depicted in Fig. 1(a). This type of waveguide has been intensively studied from the fundamental[8–12] and application[37–39] point of view, due to its ease of fabrication compared to other photonic crystal structures. In this work, the refractive index at λ_0 for air is considered to be $n_{air} = 1$ and for silicon $n_{Si} = 3.46$. Although silicon is not perfectly transparent at this wavelength, due to the absorption caused by the presence of phonon transitions, we consider a real refractive index for the sake of simplicity. Working with monochromatic waves, this lack of transparency just entails a moderate reduction in transmission, which does not affect significantly the performance of the structure considered here. The PhC lattice period is $a = 4.9\,\mu m$ and the holes radii $r = 0.48\,a$, while the silicon slab thickness is $t = 0.6\,a$. The slab is surrounded by air, in a membrane configuration. The TM-like mode supported by this structure at λ_0, depicted in Fig. 1(b), propagates along the PhC-wg with an effective wavelength of $\lambda_{PhC,TM} = 3.46\,\mu m$. The two-wire TL consists of two parallel gold wires of length $L_w = 60\,\mu m$, width $w = 200\,nm$, and thickness $h = 40\,nm$, which are separated by an air gap $g = 300\,nm$, as shown in Fig. 1(a). Gold is modeled as a Lorentz-Drude material,[40] taking into account both the dielectric function of free electrons and the absorption of light by the possible transitions of bound electrons. This model provides a refractive index of $n_{Au} = 12.59 + i\,59$ for $10\,\mu m$ wavelength. Such a large value for the imaginary part of the refractive index will be the origin of a significantly lossy behavior. The spatial field distribution $Re(E_z/E_{z,0})$ of the symmetric mode is depicted in Fig. 1(c). At the incident wavelength λ_0, the computed effective wavelength for the symmetric mode is $\lambda_{TL,s} = 3.1\,\mu m$, which is relatively close to the effective wavelength of the photonic crystal waveguide, $\lambda_{PhC,TM} = 3.46\,\mu m$. We thus expect efficient coupling, which is verified by the simulations presented next.

An input plane wave at $\lambda_0 = 10\,\mu m$ polarized along the z-direction, is set at the entrance of the PhC-wg with an initial intensity of $I_0 = 1\,(V/m)^2$. The propagation of the mid-IR light along the hybrid structure is depicted in Figs. 2 and 3, which show the normalized electric field intensity and the normalized electric field, respectively. In Fig. 2, the intensity is shown in an x-y plane at the center of the PhC-wg, and a x-z plane at the center of one of the gold wires of the TL. Note that the intensity in the x-z plane at the center of the other gold wire is analogous. All the results presented hereafter have been obtained using the finite element method (FEM)[23,25,41]

COMSOL Multiphysics. For further verification, the results obtained from FEM have been complemented with the finite differences in time domain (FDTD) method OptiFDTD.

Figures 2 and 3 illustrate how the input wave couples to the PhC-wg TM-like mode and starts propagating with an effective wavelength of $\lambda_w = 3.46\,\mu m = \lambda_{PhC,TM}$. Where the TL begins, the energy starts to be gradually transferred from the PhC-wg to the TL (marked by L_c in Fig. 2). On the TL, the effective wavelength is $\lambda_t = 3.32\,\mu m$, as measured in Figs. 3(a) and 3(b). Judging from the cross-sectional field distribution observed in Fig. 3(c), the TM-like mode of the PhC-wg couples to the symmetric mode of the TL, as it was expected since both modes present the same symmetry. As clearly seen in Fig. 2, energy transfer to the TL is complete at a distance of $L_c \approx 8\,\mu m$ from the beginning of the TL. Subsequently, the energy starts being transferred back to the center of the PhC-wg and then back again to the TL with an oscillation period of approximately $L_o \approx 18\,\mu m$. This periodic energy transfer can be understood as a beating between the photonic TM-like PhC-wg mode and the symmetric mode of the metallic TL. An analogous effect has been noticed in Refs. 24 and 25, for the cases of coupling from a dielectric ridge waveguide to a metallic slot waveguide and to a hybrid plasmonic waveguide, respectively.
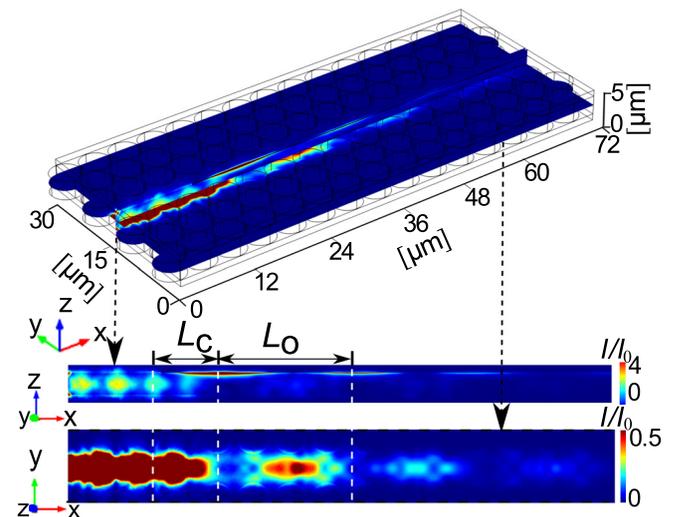
FIG. 2. Normalized electric field intensity (I/I_0): on top, a view of the hybrid structure with I/I_0 at two parallel x-z planes at the center of each wire and a x-y plane at the center of the silicon slab; below, individual views of one of the x-z planes at the center of a wire and a subsection of the x-y plane at the center of the silicon slab centered in the PhC-wg ($L_c \approx 8\,\mu m$ and $L_o \approx 18\,\mu m$).

Defining the propagation length as the distance between the start of the TL and the point where the envelope of the field amplitude in the TL has decayed by a factor $1/e$ from its maximum value, it turns out to be $L \approx 41\,\mu m$.

We estimate the enhancement of the field intensity at the TL with respect to the surface of PhC-wg in order to qualitatively determine the potential of the scheme for sensing applications. Defining the field intensity enhancement factor (IEF) as the electric field intensity around the TL at the point of maximum energy transfer, normalized to the field intensity at the surface of the PhC-wg just before the TL, we obtain IEF ≈ 53. We expect that even higher intensity enhancements could be achieved by converting the symmetric TL mode into the antisymmetric TL mode by employing a plasmonic mode converter.[35]

In order to gain insights into the physics governing such efficient coupling and into the power loss mechanisms, we calculated the x-component of the normalized Poynting vector $S_x(x) = S_x(x,y,z)/S_x(0,0,0)$. Figure 4(a) shows S_x at different cross sections x_i along a $72.25\,\mu m$-long PhC-wg (without nanowires on top of it), while Fig. 4(b) shows S_x along the hybrid structure of Fig. 1. A more detailed view of S_x around the TL is presented in Fig. 4(c). At the corners of the TL, we find a strong enhancement of S_x, which may turn out useful for the development of ultra-sensitive nanoscale sensing schemes.

In order to quantify the power loss, the Poynting vector $S_x(x)$ has been integrated over the y-z plane as a function of x, yielding the power $P(x)$ passing through the cross section in x-direction at the position x, shown in Fig. 4(d). We find that the power $P(x)$ decays exponentially in the PhC-wg, curve A in Fig. 4(d). It has been verified that the loss along

the PhC-wg is caused by radiation through the top and bottom boundaries of the silicon slab. To that end, we have computed the total power loss by subtracting the outgoing power $P(x_8)$ from the incoming power $P(x_1)$. On the other hand, we have verified that the power radiated out of the silicon slab to the air cladding and substrate practically coincides with the 100% of the total loss $P(x_1)$-$P(x_8)$. The high radiation loss obtained in the propagation along the PhC-wg is due to the proximity of the guided mode to the lightline. Note that the spatial overlapping between the PhC-wg and the TL mode is large, which is beneficial for the coupling.

The power $P(x)$ changes notably when a two-wire TL is on top of the PhC-wg, as shown by curve B in Fig. 4(d). From $x = 0\,\mu m$ to the beginning of the TL ($x = 12.25\,\mu m$), we find that $P(x)$ practically coincides with that of the PhC-wg without TL (curve A). However, for $x > 12.25\,\mu m$, the
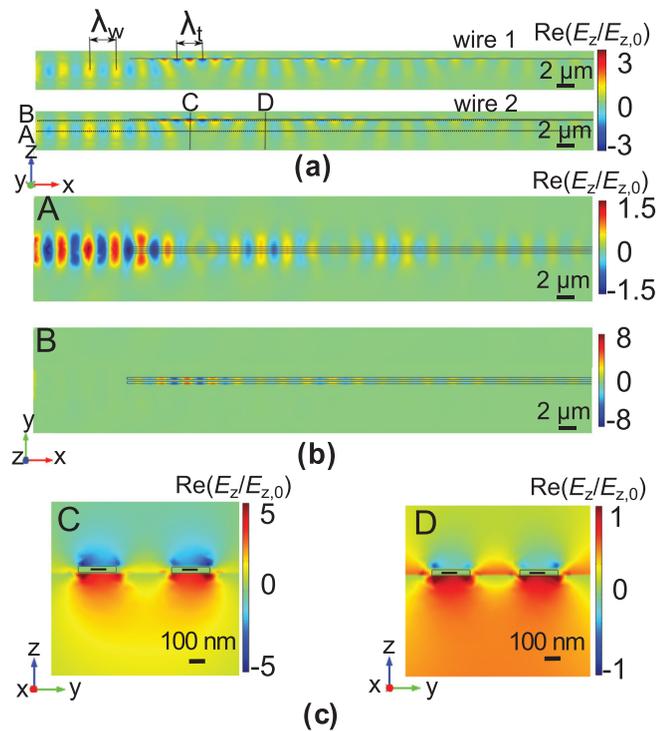
FIG. 3. Normalized real part of the electric field z-component $\mathrm{Re}(E_z/E_{z,0})$ obtained when exciting the hybrid structure with a wave polarized along z-direction in: (a) two x-z slices at half width of each gold wire, (b) x-y slices at half-height of the PhC-wg (A) and just below the TL (B); (c) y-z slices at the points of maximum (C) and minimum (D) energy transfer to the TL.
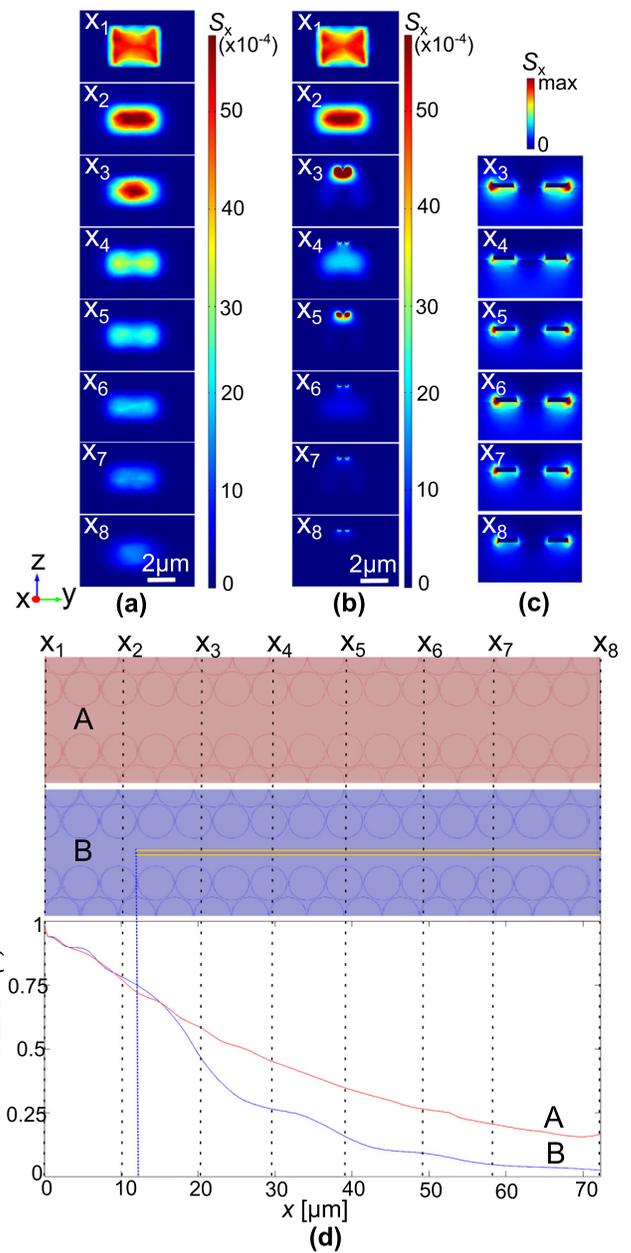
FIG. 4. Normalized Poynting vector $S_x(x)$ along x-direction (a) without TL, (b) with the metallic TL at different y-z planes (x_1-x_8), and (c) zoomed around the TL; (d) power $P(x)$ passing through the cross section in x-direction as a function of the position x without (A) and with (B) the TL.

power $P(x)$ drops significantly compared to curve A. Furthermore, we observe a slight oscillation of $P(x)$. The period of this oscillation (about $18\,\mu$m) matches that of the oscillation period of the energy transfer between the PhC-wg and the TL, $L_o \approx 18\,\mu$m. When the energy is confined in the PhC-wg, the most significant loss source is radiation to the cladding and the substrate. In the regions where the energy is confined in the TL, the most significant source of power loss is the dissipation of the surface wave in the metal. Because this dissipation is stronger than the radiation losses in the PhC-wg, the power $P(x)$ oscillates with L_o.

The inefficiencies that may arise from an imperfect coupling from the PhC-wg to the TL are minor. Defective coupling would back-reflect part of the wave energy, contributing negatively to $P(x)$ at the input PhC-wg. As it can be noticed in Fig. 4(d), the power in the initial propagation region (before the start of the TL) coincides for A and B, i.e., for the hybrid structure of Fig. 1 and for the PhC-wg alone. Therefore, the back-reflection is negligible.

Finally, we estimate the coupling efficiency by calculating the percentage of $P(x)$ coupled to the TL relative to the power $P(x = 12.25\,\mu$m) just before the TL. To that end, we calculate the power $P(x = 20.25\,\mu$m) at the position of maximum energy transfer to the TL, which turns out to be 64% of the power $P(x = 12.25\,\mu$m) entering the TL. From this percentage, almost 50% of $P(x)$ is concentrated in a small cross section of area $1400\,$nm $\times\ 500\,$nm centered in the TL. This yields a final coupling efficiency of 32%, which takes into account both the loss in the coupling region and the degree of energy concentration around the TL. In spite of the losses due to damping during the coupling, the coupling efficiency obtained here is better than the efficiencies achieved by other illumination methods[21] and within the order of magnitude of the results presented by other integrated photonic-plasmonic coupling schemes.[24,25]

This efficient coupling can be explained by using directional coupling.[36] The high fraction of power exchanged, $F = 0.64$, and the short coupling length, $L_c \sim 0.8\lambda_0$, reveal that our coupling scheme operates in the strong coupling regime, under which the coupling constant is given by $\kappa \sim \pi/2L_c$, giving rise to a value of $\kappa \sim 191\,$mm$^{-1} = 1.91/\lambda_0$. These values are comparable to the results presented recently for directional dielectric-plasmonic couplers ($F = 75\%$, $L_c \sim 0.65\lambda_0$, and $\kappa \sim 1.95/\lambda_0$).[24] This strong coupling is a direct consequence of the small phase velocity mismatch between the PhC-wg and the TL mode, given by $2\delta = \beta_{TL} - \beta_{PhC}$, where $\beta = 2\pi/\lambda_{eff}$.

In summary, we have proposed and theoretically studied the coupling from the TM-like mode of a PhC-wg to the symmetric mode of a two-wire TL in the mid-IR. A coupling efficiency of 32% is predicted together with a propagation length of $41\,\mu$m along the TL. The intensity enhancement factor at the surface of the TL with respect to the surface of the PhC-wg is $\sim$53. Using numerical calculations and the directional coupling theory, we have shown that this strong coupling is a direct consequence of the small phase velocity mismatch and the sufficient spatial overlapping between the PhC-wg and the TL modes. The simulations suggest that the coupling efficiency is limited primarily by radiation and absorption along the coupling length, a practical limitation which can be overcome by further design advances. Given the promising coupling efficiency and intensity enhancement factor, hybrid structures comprising TLs on PhC-wgs have the potential of becoming a basic building block for waveguide sensors in the mid-IR.

[1]N. Engheta, Science **317**, 1698–1702 (2007).
[2]D. Miller, Proc. IEEE **97**, 1166–1185 (2009).
[3]P. Debackere, S. Scheerlinck, P. Bienstman, and R. Baets, Opt. Express **14**(16), 7063–7072 (2006).
[4]J. Eid, A. Fehr, J. Gray, K. Luong, J. Lyle, G. Otto, P. Peluso, D. Rank, and P. Baybayan, Science **323**, 133–138 (2009).
[5]D. E. Chang, A. S. Sorensen, E. A. Demler, and M. D. Lukin, Nat. Phys. **3**, 807–812 (2007).
[6]A. Quandt, M. Ferrari, and G. C. Righini, in *New Trends in Nanotechnology and Fractional Calculus Applications* (Springer, New York, 2010), pp. 25–41.
[7]A. Mekis, J. C. Chen, I. Kurland, S. Fan, P. R. Villeneuve, and J. D. Joannopoulos, Phys. Rev. Lett. **77**, 3787–3790 (1996).
[8]T. Krauss, J. Phys. D: Appl. Phys. **40**, 2666–2670 (2007).
[9]M. Settle, M. Salib, A. Michaeli, and T. F. Krauss, Opt. Express **14**, 2440–2445 (2006).
[10]J. Li, L. O'Faolain, S. A. Schultz, and T. F. Krauss, Photonics Nanostruct. Fundam. Appl. **10**, 589–593 (2012).
[11]E. Kuramochi, M. Notomi, S. Hughes, A. Shinya, T. Watanabe, and L. Ramunno, Phys. Rev. B **72**, 161318(R) (2005).
[12]S. Maier, *Plasmonics: Fundamentals and Applications* (Springer, 2007).
[13]S. A. Maier, P. G. Kik, H. A. Atwater, S. Meltzer, E. Harel, B. E. Koel, and A. A. G. Requicha, Nature Mater. **2**, 229–232 (2003).
[14]H. Ditlbacher, A. Hohenau, D. Wagner, U. Kreibig, M. Rogers, F. Hofer, F. R. Aussenegg, and J. R. Krenn, Phys. Rev. Lett. **95**, 257403 (2005).
[15]M. Schnell, P. Alonso-González, L. Arzubiaga, F. Casanova, L. E. Hueso, A. Chuvilin, and R. Hillenbrand, Nature Photon. **5**, 283–287 (2011).
[16]S. M. García-Blanco, M. Pollnau, and S. I. Bozhevolnyi, Opt. Express **19**, 25298–25311 (2011).
[17]R. F. Oulton, V. J. Sorger, D. A. Genov, D. F. Pile, and X. Zhang, Nature Photon. **2**, 496–500 (2008).
[18]D. Dau and S. He, Opt. Express **17**, 16646–16653 (2009).
[19]L. Pyatt, B. Wiley, Y. Xia, A. Chen, and L. Dalton, Nat. Nanotechnol. **3**, 660–665 (2008).
[20]J. Mu, L. Chen, X. Li, W. P. Huang, L. C. Kimerling, and J. Michel, Appl. Phys. Lett. **103**, 131107 (2013).
[21]R. Wan, F. Liu, X. Tang, Y. Huang, and J. Peng, Appl. Phys. Lett. **94**, 141104 (2009).
[22]F. Liu, R. Wan, Y. Li, Y. Huang, Y. Miura, D. Ohnishi, and J. Peng, Appl. Phys. Lett. **95**, 091104 (2009).
[23]F. Liu, Y. Li, R. Wan, Y. Huang, X. Feng, and W. Zhang, J. Lightwave Technol. **29**, 1265–1273 (2011).
[24]C. Delacour, S. Blaize, P. Grosse, J. M. Fedeli, A. Bruyant, R. Salas-Montiel, G. Lerondel, and A. Chelnokov, Nano Lett. **10**, 2922–2926 (2010).

[25]Y. Song, J. Wang, Q. Li, M. Yan, and M. Qiu, Opt. Express **18**, 13173–13179 (2010).

[26]M. L. Nesterov, A. V. Kats and S. K. Turitsyn, Opt. Express **16**, 20227–20240 (2008).

[27]A. Bousseksou, A. Babuty, J.-P. Tetienne, I. Moldovan-Doyen, R. Braive, G. Beaudoin, I. Sagnes, Y. De Wilde, and R. Colombelli, Opt. Express **20**, 13738–13747 (2012).

[28]P. Krenz, R. Olmon, B. Lail, M. Raschke, and G. Boreman, Opt. Express **18**, 21678–21686 (2010).

[29]R. Stanley, "Plasmonics in the mid-infrared," Nature Photon. **6**, 409–411 (2012).

[30]S. Law, D. C. Adams, A. M. Taylor, and D. Wasserman, Opt. Express **20**, 12155–12165 (2012).

[31]A. C. Jones, R. L. Olmon, S. E. Skrabalak, B. J. Wiley, Y. N. Xia, and M. B. Raschke, Nano Lett. **9**, 2553–2558 (2009).

[32]D. S. Ly-Gagnon, K. C. Balram, J. S. White, P. Wahl, M. L. Brongersma, and D. A. B. Miller, Nanophotonics **1**, 9–16 (2012).

[33]Y. Hung, C. Huang, and J. S. Huang, Opt. Express **20**, 20342–20355 (2012).

[34]R. Soref, Nature Photon. **4**, 495–497 (2010).

[35]R. Shankar, R. Leijssen, I. Bulu, and M. Lončar, Opt. Express **19**, 5579–5586 (2011).

[36]D. K. Gramotnev, K. C. Vernon, and D. F. P. Pile, Appl. Phys. B **93**, 99–106 (2008).

[37]C. Jamois, R. B. Wehrspohna, L. C. Andreanic, C. Hermannd, O. Hessd, and U. Göselea, Photonics Nanostruct. Fundam. Appl. **1**, 1–13 (2003).

[38]C. Husko, T. D. Vo, B. Corcoran, J. Li, T. F. Krauss, and B. J. Eggleton, Opt. Express **19**, 20681–20690 (2011).

[39]N. Skivesen, A. Têtu, M. Kristensen, J. Kjems, L. H. Frandsen, and P. I. Borel, Opt. Express **15**(6), 3169–3176 (2007).

[40]E. D. Palik, *Handbook of Optical Constants of Solids* (Academic Press, 1998).

[41]I. Andonegui and A. J. Garcia-Adeva, Opt. Express **21**, 4072–4092 (2013).